

1 Ocean-eddy dissipation estimates at the Atlantic
2 zonal boundaries

C. J. Wright,¹ R.B. Scott,¹ B.K. Arbic,² and D. F. Furnival¹

B. K. Arbic, Department of Geological Sciences, University of Michigan, Ann Arbor, Michigan, United States (arbic@umich.edu)

D. F. Furnival, Laboratoire de Physique des Océans, Université de Bretagne Occidentale, Brest, France (darran.furnival@univ-brest.fr)

R. B. Scott, Laboratoire de Physique des Océans, Université de Bretagne Occidentale, Brest, France (robert.scott@univ-brest.fr)

C. J. Wright, Laboratoire de Physique des Océans, Université de Bretagne Occidentale, Brest, France (corwin.wright@univ-brest.fr)

¹Laboratoire de Physique des Océans,
Université de Bretagne Occidentale, Brest,
France

²Department of Geological Sciences,
University of Michigan, Ann Arbor,
Michigan

3 **Abstract.** Estimates of the eddy dissipation due to bottom boundary layer
4 drag at the eastern and western boundaries of the North Atlantic ocean are
5 computed using data from the world's largest archive of ocean current me-
6 ter time series. We show from these data that a significant proportion of such
7 loss in this region is due to dissipation at the western boundary ocean floor
8 via quadratic bottom boundary layer drag, with an estimated 40–60% (31–
9 47 GW) of the wind input power across the whole basin dissipated by this
10 method. We further show that the majority of this dissipation occurs at shal-
11 low depths, <500 m; this has significant implications for the power available
12 for abyssal mixing.

1. Introduction

13 The majority of the mechanical energy in the deep ocean is carried by currents with
14 horizontal lengthscales of at least tens of kilometers and timescales of multiple days. The
15 source of this energy — wind acting on the ocean surface — is well-known and well-
16 constrained [*Wunsch, 1998; Scott, 1999a, b; Hughes and Wilson, 2008; Scott and Xu,*
17 *2009*], but the mechanisms by which it is balanced by dissipation are poorly understood
18 [*Ferrari and Wunsch, 2009; Wunsch and Ferrari, 2004*]. This has significance for the
19 general oceanic circulation: a better understanding of the underlying mechanisms would
20 allow us to locate mixing processes within the vertical water column, providing an im-
21 portant constraint on the meridional overturning circulation [*Munk and Wunsch, 1998*].
22 Recent studies [*Scott et al., 2011*] have shown that dissipation in the southern hemisphere
23 occurs primarily through topographic lee wave generation, but this is a comparatively
24 small effect in the northern hemisphere, dissipating only around 10% (8.1 GW) of the
25 wind power input to the North Atlantic.

26 Several mechanisms have been suggested for the removal of this eddy energy from the
27 oceans, which can be divided broadly into two main categories: instability and wave
28 processes acting in the interior of the water column [e.g. *Bühler and McIntyre, 2005;*
29 *Molemaker et al., 2005; Zhai et al., 2010*] and bottom boundary layer (BBL) drag processes
30 [e.g. *Weatherly, 1984; Sen et al., 2008; Arbic et al., 2009*]. Suppression by the surface winds
31 can also be included as a third category [*Scott and Xu, 2009; Zhai and Greatbatch, 2007*],
32 but is in practice already accounted for in the net input energy from the wind. This net

33 input energy can be calculated using the method of *Scott and Xu* [2009] as around 80GW
34 for the North Atlantic basin as a whole.

35 It has recently been shown that the removal of this energy in the northern hemisphere
36 takes place primarily at the western boundary: eddies propagate westwards at the speed
37 of Rossby waves [*Chelton et al.*, 2007; *Kanzow et al.*, 2009] leading to heightened eddy
38 kinetic energy levels [*Kanzow et al.*, 2009; *Shum et al.*, 1990] and resulting eddy dissipation
39 [*Sen et al.*, 2008; *Arbic et al.*, 2009; *Zhai et al.*, 2010] at the boundary, which is then lost to
40 the system [*Wunsch and Ferrari*, 2004]. *Zhai et al.* [2010], using a combination of models,
41 satellite altimetry, and climatological hydrographic data, estimate a sink $\sim 22\text{--}39$ GW for
42 the Atlantic north of $\phi=10^\circ$ due to a flux of mechanical energy into the western boundary
43 region, and speculate that this is due to excitation of turbulence in the interior of the
44 water column, which would potentially make this turbulence available to drive abyssal
45 mixing. However, there are alternative mechanisms which may better explain this loss.
46 *Arbic et al.* [2009], using the Parallel Ocean Program model, estimated a quadratic BBL
47 dissipation sink of 28-69 GW in the shallow ($<1000\text{m}$) North Atlantic and 48-120 GW in
48 the North Atlantic at all depths, with a large proportion of this in the western boundary.
49 These dissipation rates are large enough to account for the flux of mechanical energy into
50 the western boundary layer estimated by *Zhai et al.* and suggest that this is an important
51 contributing mechanism. If so, this would leave little if any of the 80GW of the North
52 Atlantic wind power input available to drive abyssal mixing in the important western
53 boundary region [*Scott and Marotzke*, 2002].

54 By using a collection of ocean current time series derived from the oceanographic re-
55 search programmes of multiple countries, we are able to experimentally quantify the energy

56 lost due to eddy dissipation via quadratic BBL drag ('BBL dissipation') at the western
57 boundary of the North Atlantic, and to contrast this with the equivalent values for the
58 eastern boundary and with the results of previous studies.

2. Methods

2.1. Time Series Data

59 Our time series data are derived from the Global Multi-Archive Current Meter Database
60 (GMACMD) [Scott *et al.*, 2010, 2011]. This is a global collection of (at time of writing)
61 approximately 47 000 physical oceanographic time series, primarily derived from ocean
62 current meters, converted into a standard format.

63 The current meters used for our analysis are those which fall within the geographic
64 regions outlined below and within the bottom 10% of the ocean. Shelf regions, defined
65 as those with a depth less than 100 m are excluded, as are current meters within 10 m of
66 the ocean bottom. Meters with less than 30 days of data are excluded from our analysis;
67 the bulk of time series are between six months and a year in length, with the longest
68 lasting for slightly over three years. Many current meter moorings hold multiple meters
69 at different depths; where this is the case, only the deepest current meter is considered.
70 Six extreme-outliers, lying more than 5 standard deviations above the overall mean for
71 both regions, have also been excluded from our analysis. All velocity time series used
72 have been regularised to a common three-hour time step between measurements; series
73 with either an irregular timestep or a timestep shorter than this have been averaged to
74 this value, whilst series with a longer timestep have been discarded.

2.2. Regions

75 We define the eastern and western boundaries as the region within 700 km of the shore-
76 line between 15N and 60N; this criterion maximises available coverage of measurements,
77 while still including regions with a sufficient range of depths to allow assessment of the
78 eddy dissipation as a function of depth. We assess the western and eastern boundaries
79 separately.

80 Allowing for these and the above considerations, 402 time series (289 on the western
81 boundary, 113 on the eastern boundary) are used. These locations are shown as crosses on
82 figure 1; their highly uneven distribution should be noted. Also shown on this figure are
83 the areas enclosed within one decorrelation scale δ of these measurements (solid contours;
84 see below). Currents within $\delta \leq 1$ are assumed to be well-correlated with the values at
85 the measurement location. Around 26% of the western and 20% of the eastern boundary
86 regions are within $\delta \leq 1$ of our measurements (see table 1) .

87 The measurements used may exhibit a bias in their measured currents, and hence their
88 BBL drag, due to their selection as places of interest for current measurements [*Sen*,
89 *et al.*, 2008; *Holloway et al.*, 2011]; accordingly, the extrapolation beyond the directly-
90 measured region is uncertain. Estimates based on model and satellite data (see section
91 4.2) suggest a potential negative bias in BBL dissipation due to this extrapolation of
92 5–20% on the eastern boundary and a potential positive bias of 0–50% on the western
93 boundary. Nevertheless, the values for $\delta \leq 1$ can be considered to be accurate, and hence
94 will form a sensible lower bound on the BBL dissipation.

2.3. Decorrelation Scales

The longitudinal and latitudinal decorrelation scales δ_θ and δ_ϕ respectively are defined as [Ducet et al., 2000]

$$\delta_\theta = \delta_\phi = 50 + 250 \left(\frac{900}{900 + 2\phi^2} \right) \text{ km.} \quad (1)$$

and the vertical decorrelation scale as

$$\delta_z = \left(\frac{f}{N} \right) \left(\frac{2}{\delta_\theta^{-1} + \delta_\phi^{-1}} \right), \quad (2)$$

where N is the Brunt-Väisälä frequency and f the Coriolis parameter. Values of N are determined from the WOA2009 seasonal temperature and salinity climatology using equation 3.71 of Gill [1982] and averaged over the seasons, omitting negative values. The values for δ_θ , δ_ϕ and δ_z are then summed in quadrature to give an overall measure for decorrelation length δ at a given grid point

$$\delta = \sqrt{\left(\frac{\Delta\phi}{\delta_\phi} \right)^2 + \left(\frac{\Delta\theta}{\delta_\theta} \right)^2 + \left(\frac{\Delta z}{\delta_z} \right)^2}, \quad (3)$$

95 where $\Delta\phi$ represents the latitudinal distance between the grid point and the meter in the
 96 same units as δ_ϕ , etc. δ is hence dimensionless.

2.4. BBL Dissipation

BBL dissipation results from quadratic BBL momentum drag, parameterized as a term

$$\frac{\rho c_d \sqrt{u^2 + v^2} \mathbf{u}}{H}$$

where $\rho = 1035$ is the mean density sea water density, $c_d = 0.0025$ is the quadratic bottom drag coefficient, $\mathbf{u} = (u, v)$ is the background flow velocity above the BBL, and H is the BBL thickness. Taking the inner product with \mathbf{u} and integrating over H , we obtains the

standard formula for quadratic BBL dissipation,

$$\rho c_d |\mathbf{u}|^3.$$

97 To focus on the dissipation of the subinertial, essentially geostrophic, flow, D_e , requires
 98 some care because of the nonlinearity of the dissipation on flow velocity. The formula for
 99 D_e that retains the dissipation due to interaction between high and low frequencies, is

$$D_e = \rho c_d \langle \sqrt{u^2 + v^2} \mathbf{u} \rangle \cdot \langle \mathbf{u} \rangle \quad (4)$$

100 where $\langle x \rangle$ is the low-pass filter of time series x , here a Butterworth filter with 3-day
 101 cutoff. For interest we also isolated the dissipation due to interaction between high and
 102 low frequencies,

$$\rho c_d \langle \sqrt{u^2 + v^2} \mathbf{u} \rangle \cdot \langle \mathbf{u} \rangle - \rho c_d |\langle \mathbf{u} \rangle|^3 \quad (5)$$

103 and found it to generally be around 15% of the D_e in shallow seas where the tides were
 104 strong, and less in the deep ocean thus justifying the omission of this component of the
 105 dissipation in previous studies [*Sen et al.*, 2008; *Arbic et al.*, 2009].

2.5. Analysis

106 We compute the time-mean value of D_e (per unit area; Wm^{-2}) at each measurement lo-
 107 cation, and then extrapolate these values to cover the entire area on a regular $0.25^\circ \times 0.25^\circ$
 108 grid. For each gridpoint, we assign a value of D_e equal to the value of the nearest mea-
 109 surement, defined as that the smallest multiple of δ away. This may not be the closest
 110 measurement geographically, as the calculation of δ is z -weighted; accordingly, a measure-
 111 ment at a similar depth may be selected in preference to one geographically closer but at
 112 a very different depth.

3. Results

3.1. Geographic

Figure 2 shows estimates for the BBL dissipation. The first key result observed is that estimated values are significantly lower in the eastern boundary region (figure 2(b)) than in the western boundary region (figure 2(a)); values observed in the eastern boundary, with the exception of some small outlier regions around the British Isles which reach up to 50 mWm^{-2} , peak at $\sim 10 \text{ mWm}^{-2}$, whilst values on the western boundary are larger in general, with an absolute peak near Florida at $\sim 80 \text{ mWm}^{-2}$, around 25 mWm^{-2} above the absolute peak on the eastern boundary. The highest values on the eastern boundary south of the English Channel reach no higher than 3 mWm^{-2} ; in contrast, high values are observed along the entire western boundary, with particular peaks around Florida, east of the coast of Labrador, and in the Gulf Stream near $\sim (41\text{N}, 52\text{W})$. These peaks are consistent with the effects of the strong western boundary current.

3.2. By Depth

Figure 3 shows the same results, divided up by δ (separate plots) and depth (horizontal axis, in 500 m bins). The wide bars show area, narrow bars total estimated BBL dissipation, and the line measured BBL dissipation per unit area D_e . We also obtain summed values over all depths (Table 1).

Figures 3(a) and 3(b) show results for $\delta \leq 1$, i.e. the region which should be well-correlated with our measurement locations, and hence the most confident results. We observe in both regions that the highest measured values of unnormalised BBL dissipation occur in the shallowest regions, with secondary peaks at high depths. In the western boundary this secondary peak is at depths below $\sim 3 \text{ km}$; this is consistent with the intense

133 and more depth-independent flow of Gulf Stream eddies observed by *Schmitz and Luyten*
134 [1991], which presumably barotropise through nonlinear interactions. In contrast, the
135 eastern boundary shows a much smaller secondary peak at depths below 4 km, with values
136 otherwise declining with depth. Normalised dissipation shows high values at high depths
137 on the western boundary, but as total area is small here compared to the shallower regions
138 this makes a comparatively small contribution to the total. 15.0 GW is estimated for $\delta \leq 1$
139 on the western boundary against 2.5 GW on the eastern; while the area within $\delta \leq 1$ on
140 the western boundary is around thrice that on the eastern, this is still a massive imbalance,
141 consistent with the significantly greater energy loss expected at the western boundary.

142 As discussed above, the results for $\delta \leq 1$ provide an accurate lower bound on the BBL
143 dissipation estimates, whereas our extrapolation from this value may be positive-biased:
144 it is hence important to note that the estimated dissipation in this third of the total
145 western boundary area region makes up nearly 70% of Zhai et al's lower bound of 22 GW.
146 On this boundary, around 40% of the estimated dissipation is at shallow depths, <1 km;
147 while there is substantial dissipation per unit area in the deeper regions, the actual area
148 at these depths is small, leading to an overall contribution of around 30% of measured
149 BBL dissipation in the western boundary from depths >4 km. This is not the case in
150 the eastern boundary: while dissipation declines with increasing depth, there is no single
151 depth range which dominates in the way we see in the west.

152 The lower row of figure 3 shows extrapolated results for the entire region on both
153 boundaries. Distributions observed are broadly similar to those measured for $\delta \leq 1$; in
154 the eastern boundary, most BBL dissipation is in shallower regions, whilst in the western
155 boundary there is a substantial secondary peak at high depth. Total BBL dissipation

156 for the two boundary regions is again sharply different: for the all-locations case, BBL
157 dissipation in the eastern boundary totals 9.3 GW compared to 47.0 GW for the western
158 boundary. Given our estimated positive bias and their expected negative bias, this is
159 comparable to the $\sim 22\text{--}39$ GW estimated by *Zhai et al.* [2010] for the sink of eddy energy
160 in the North Atlantic, and hence suggests that bottom boundary layer dissipation may be
161 one of the dominant processes acting to dissipate eddies here. It also compares favourably
162 to the results of *Arbic et al.* [2009], with the two regions totalling 56.3 GW compared
163 to their range of 48-120 GW for whole North Atlantic basin. Again, while there is a
164 substantial secondary peak of D_e , the bulk of the measured BBL dissipation is in the
165 shallow regions, again consistent with *Arbic et al.* The proportion of dissipation in the
166 extrapolated areas of the western boundary is broadly similar to that within $\delta < 1$, with
167 around 50% at depths < 1 km and around 10% at depths > 4 km.

4. Discussion

4.1. Errors - Statistical

168 For the directly-measured $\delta \leq 1$ region, a statistical bootstrapping process is used. For
169 each individual time series, we compute ten-day non-overlapping means of the BBL dis-
170 sipation D_e . This criterion of ten days is determined by an analysis of the time taken
171 for each series to auto-decorrelate: $\sim 90\%$ of the time series auto-decorrelate within this
172 time. We then select all gridpoints on our 0.25×0.25 degree grid which lie within $\delta \leq 1$ of
173 a measurement location, and subdivide by depth; for each 500 m depth bin, we select all
174 contributing time series, area-weight them appropriately, and then statistically bootstrap
175 the mean of each ten-day-averaged area-weighted series one thousand times to obtain es-
176 timates of the BBL dissipation due to that series. For each of the thousand trials, we

177 then sum over all the contributing area-weighted series, obtaining a distribution of one
178 thousand total BBL dissipation values for each depth bin, and select the 95% confidence
179 interval. This is indicated on panels (a) and (b) of figure 3 by the whiskered lines for
180 each dissipation bar. No uncertainty is indicated on the area bars as these values are
181 well-known.

4.2. Errors - Extrapolation

182 The bootstrapping method was not used for our extrapolation to the full area, as the ef-
183 fects due to statistical variability were considered to be less than the inherent uncertainty
184 introduced to the extrapolation by the uneven distribution of the measurement locations.
185 As such, statistically-derived uncertainties on these results would convey a false sense of
186 the true uncertainty. Instead, to assess the biases on our extrapolation to the full area,
187 comparisons to model (HYCOM, *Chassignet et al.* [2007]) data and satellite altimeter
188 (Collecte Localisation Satellites, *Ducet et al.* [2000]) data for the ocean surface were per-
189 formed. These data are regularly-gridded over the whole basin, and should not suffer an
190 especial bias towards any individual region: thus, while there may be inherent differences
191 in the magnitudes computed via these methods, the ratio between the total values for the
192 measured and extrapolated areas is useful as an estimate of the bias introduced by the
193 locations of our measurements.

194 Each dataset was interpolated to the same 0.25×0.25 degree grid used in our analysis,
195 and the same spatial selection criteria (latitude and distance from coast) applied; mean
196 dissipations for the region within $\delta \leq 1$ of a current meter and the whole region were
197 then computed and compared. Results were computed separately for the east and west
198 boundaries as a ratio of the mean for the whole region to the mean for the region where

199 $\delta \leq 1$; a value less than 1 indicates that an extrapolation from $\delta \leq 1$ to the whole region
200 will be negative-biased and vice versa

201 For the eastern boundary, both the model and satellite studies suggest that our results
202 slightly underestimate the result, with ratios of 1.0 and 0.8 for the satellite and model
203 results respectively. This implies that values on the eastern boundary may be up to
204 20% higher than we estimate. For the western boundary, the results are slightly more
205 divergent: the model gives a ratio of 1.0, whilst the satellite gives a ratio 1.5; that is to
206 say, according to the model bias calculation, our extrapolation should continue to give an
207 accurate result, whilst the satellite analysis suggests that we may be overstating the result
208 by 50%. Examination of the results for the two datasets suggests that this is primarily
209 due to a difference in the regions that dominate their speed distributions: for the satellite
210 study, which uses surface data, the highest speeds on the western boundary are in the
211 region where the Gulf Stream is separated from the continent, whilst for the model study,
212 where the deepest model level was used, the highest velocities are recorded off the coast of
213 South Carolina and Georgia in a region where our measurements are denser. Hence, our
214 extrapolation bias on this boundary is expected to be better represented by the model
215 analysis than by the satellite analysis, accordingly suggesting a bias towards the lower
216 end of this distribution. In the text, however, we conservatively allow for the significant
217 difference implied by the satellite results.

218 For comparison, the model results estimate WBL dissipation as 33.6 GW and EBL dissi-
219 pation as 1.4 GW, also highlighting the strong difference on the two boundaries. Satellite
220 results are very different since they measure the much-faster surface currents, and are
221 accordingly not presented.

5. Conclusions

222 Based upon our results, we conclude that BBL dissipation is a major route of eddy
223 dissipation in the North Atlantic, with eddy energy primarily dissipated at shallow depths
224 on the western boundary but also in significant amounts in deeper regions. Losses via this
225 route potentially amount to 40–60% (31–47 GW) of the 80GW input from wind working
226 on the subinertial surface currents of the North Atlantic. We further estimate that around
227 40% of the western boundary BBL dissipation occurs in regions with seafloor depth < 1 km
228 of the ocean; depths <1 km comprise significantly more than half of measured dissipation
229 in the western boundary. This is consistent with the substantial impact of current velocity
230 on BBL dissipation, $\propto |\mathbf{u}|^3$; mid-ocean Rossby waves are surface-intensified and can thus
231 propagate with little bottom dissipation, but when entering shallower regions, the resulting
232 bottom velocities lead to very high dissipation. This has significant implications for mixing
233 in the North Atlantic; energy dissipated in shallower regions will be unavailable for deep-
234 ocean mixing, leaving the source of the power required to drive these processes ambiguous.

235 **Acknowledgments.** CJW was funded by a Stratégie d’Attractivité Durable award
236 from the Région Bretagne through the Université de Bretagne Occidentale. RBS acknowl-
237 edges funding provided by NSF grant OCE-0526412 and OCE-0851457, a contract with
238 the National Oceanography Centre, Southampton, UK. BKA was supported by United
239 States National Science Foundation grant OCE-09607820.

References

240 Arbic, B. K., et al. (2009), Estimates of bottom flows and bottom boundary layer dissi-
241 pation of the oceanic general circulation from global high-resolution models, *Journal of*

- 242 *Geophysical Research*, 114(C2), C02,024+, doi:10.1029/2008JC005072.
- 243 Bühler, O., and M. E. McIntyre (2005), Wave capture and wave-vortex duality, *Journal*
244 *of Fluid Mechanics*, 534, 67–95, doi:10.1017/S0022112005004374.
- 245 Chassignet, E. P., H. E. Hurlburt, O. M. Smedstad, G. R. Halliwell, P. J. Hogan, A. J.
246 Wallcraft, R. Baraille, and R. Bleck (2007), The HYCOM (HYbrid Coordinate Ocean
247 Model) data assimilative system, *Journal of Marine Systems*, 65(1-4), 60–83, doi:
248 10.1016/j.jmarsys.2005.09.016.
- 249 Chelton, D. B., M. G. Schlax, R. M. Samelson, and R. A. de Szoeke (2007), Global
250 observations of large oceanic eddies, *Geophysical Research Letters*, 34(15), L15,606,
251 doi:10.1029/2007GL030812.
- 252 Ducet, N., P. Y. Le Traon, and G. Reverdin (2000), Global high-resolution mapping of
253 ocean circulation from TOPEX/Poseidon and ERS-1 and -2, *Journal of Geophysical*
254 *Research*, 105(C8), doi:10.1029/2000JC900063.
- 255 Ferrari, R., and C. Wunsch (2009), Ocean Circulation Kinetic Energy: Reser-
256 voirs, Sources, and Sinks, *Annual Review of Fluid Mechanics*, 41(1), 253–282, doi:
257 10.1146/annurev.fluid.40.111406.102139.
- 258 Gill, A. E. (1982), *Atmosphere-ocean dynamics*, International geophysics series, Academic
259 Press.
- 260 Holloway, G., A. T. Nguyen, and Z. Wang (2011), Oceans and ocean models as seen by
261 current meters, *Journal of Geophysical Research*, doi:10.1029/2011JC007044, in Press.
- 262 Hughes, C. W., and C. Wilson (2008), Wind work on the geostrophic circulation: an
263 observational study of the effect of small scales in the wind stress, *J. Geophys. Res.*,
264 113, C02,016.

- 265 Kanzow, T., H. L. Johnson, D. P. Marshall, S. A. Cunningham, Hirschi, A. Mujahid, H. L.
266 Bryden, and W. E. Johns (2009), Basinwide Integrated Volume Transports in an Eddy-
267 Filled Ocean, *J. Phys. Oceanogr.*, *39*(12), 3091–3110, doi:10.1175/2009JPO4185.1.
- 268 Molemaker, M. J., J. C. McWilliams, and I. Yavneh (2005), Baroclinic Instability and
269 Loss of Balance, *J. Phys. Oceanogr.*, *35*(9), 1505–1517, doi:10.1175/JPO2770.1.
- 270 Munk, W., and C. Wunsch (1998), Abyssal recipes II: energetics of tidal and wind mixing,
271 *Deep Sea Research Part I: Oceanographic Research Papers*, *45*(12), 1977–2010, doi:
272 10.1016/S0967-0637(98)00070-3.
- 273 Schmitz, W. J., and J. R. Luyten (1991), Spectral time scales for mid-latitude eddies,
274 *Journal of Marine Research*, pp. 75–107, doi:10.1357/002224091784968585.
- 275 Scott, J. R., and J. Marotzke (2002), The Location of Diapycnal Mixing and the
276 Meridional Overturning Circulation, *J. Phys. Oceanogr.*, *32*(12), 3578–3595, doi:
277 10.1175/1520-0485(2002)032%3C3578:TLODMA%3E2.0.CO;2.
- 278 Scott, R. B. (1999a), Mechanical energy flux to the surface geostrophic flow using
279 TOPEX/poseidon data, in *23rd EGS General Assembly, Physics and Chemistry of the*
280 *Earth Part A – Solid Earth and Geodesy*, vol. 24, pp. 399–402, European Geophysical
281 Society, Nice, France.
- 282 Scott, R. B. (1999b), Geostrophic energetics and the small viscosity behaviour of an
283 idealized ocean circulation model, Ph.d. dissertation, McGill University, Montreal, PQ,
284 [Available from <http://www.ig.utexas.edu/people/staff/rscott/>].
- 285 Scott, R. B., and Y. Xu (2009), An update on the wind power input to the surface
286 geostrophic flow of the World Ocean, *Deep Sea Research Part I: Oceanographic Research*
287 *Papers*, *56*(3), 295–304, doi:10.1016/j.dsr.2008.09.010.

- 288 Scott, R. B., B. K. Arbic, E. P. Chassignet, A. C. Coward, M. Maltrud, W. J. Merryfield,
289 A. Srinivasan, and A. Varghese (2010), Total kinetic energy in four global eddying ocean
290 circulation models and over 5000 current meter records, *Ocean Modelling*, *32*(3-4), 157–
291 169, doi:10.1016/j.ocemod.2010.01.005.
- 292 Scott, R. B., J. A. Goff, A. C. N. Garabato, and A. J. G. Nurser (2011), Global
293 rate and spectral characteristics of internal gravity wave generation by geostrophic
294 flow over topography, *Journal of Geophysical Research*, *116*(C9), C09,029+, doi:
295 10.1029/2011JC007005.
- 296 Sen, A., R. B. Scott, and B. K. Arbic (2008), Global energy dissipation rate of deep-ocean
297 low-frequency flows by quadratic bottom boundary layer drag: Computations from
298 current-meter data, *Geophysical Research Letters*, *35*(9), doi:10.1029/2008GL033407.
- 299 Shum, C. K., R. A. Werner, D. T. Sandwell, B. H. Zhang, R. S. Nerem, and B. D. Tapley
300 (1990), Variations of Global Mesoscale Eddy Energy Observed From Geosat, *Journal*
301 *of Geophysical Research*, *95*(C10), doi:10.1029/JC095iC10p17865.
- 302 Weatherly, G. L. (1984), An estimate of bottom frictional dissipation by Gulf Stream fluc-
303 tuations, *Journal of Marine Research*, pp. 289–301, doi:10.1357/002224084788502729.
- 304 Wunsch, C. (1998), The Work Done by the Wind on the Oceanic Gen-
305 eral Circulation, *J. Phys. Oceanogr.*, *28*(11), 2332–2340, doi:10.1175/1520-
306 0485(1998)028%3C2332:TWDBTW%3E2.0.CO;2.
- 307 Wunsch, C., and R. Ferrari (2004), Vertical mixing, energy and the general cir-
308 culation of the oceans, *Annual Review of Fluid Mechanics*, *36*(1), 281–314, doi:
309 10.1146/annurev.fluid.36.050802.122121.

Table 1. Key data for the two regions considered. ‘ D_e ’ indicates the total BBL dissipation measured in GW, ‘A’ the total area in thousands of square kilometers, and ‘%’ the proportion of the total area. Results are shown for distances within 1 decorrelation scale δ of a current meter and extrapolated over the whole region.

Region	Time Series	$\delta \leq 1$			All locations		
		D_e	A	%	D_e	A	%
Western	289	15.0	2400	32.1	47.0	6880	100
Eastern	113	2.5	790	18.1	9.3	4320	100

- 310 Wyrтки, K., L. Magaard, and J. Hager (1976), Eddy Energy in the Oceans, *Journal of*
311 *Geophysical Research*, 81(15), doi:10.1029/JC081i015p02641.
- 312 Zhai, X., and R. J. Greatbatch (2007), Wind work in a model of the northwest Atlantic
313 Ocean, *Geophysical Research Letters*, 34(4), L04,606, doi:10.1029/2006GL028907.
- 314 Zhai, X., H. L. Johnson, and D. P. Marshall (2010), Significant sink of ocean-eddy energy
315 near western boundaries, *Nature Geoscience*, 3(9), 608–612, doi:10.1038/ngeo943.

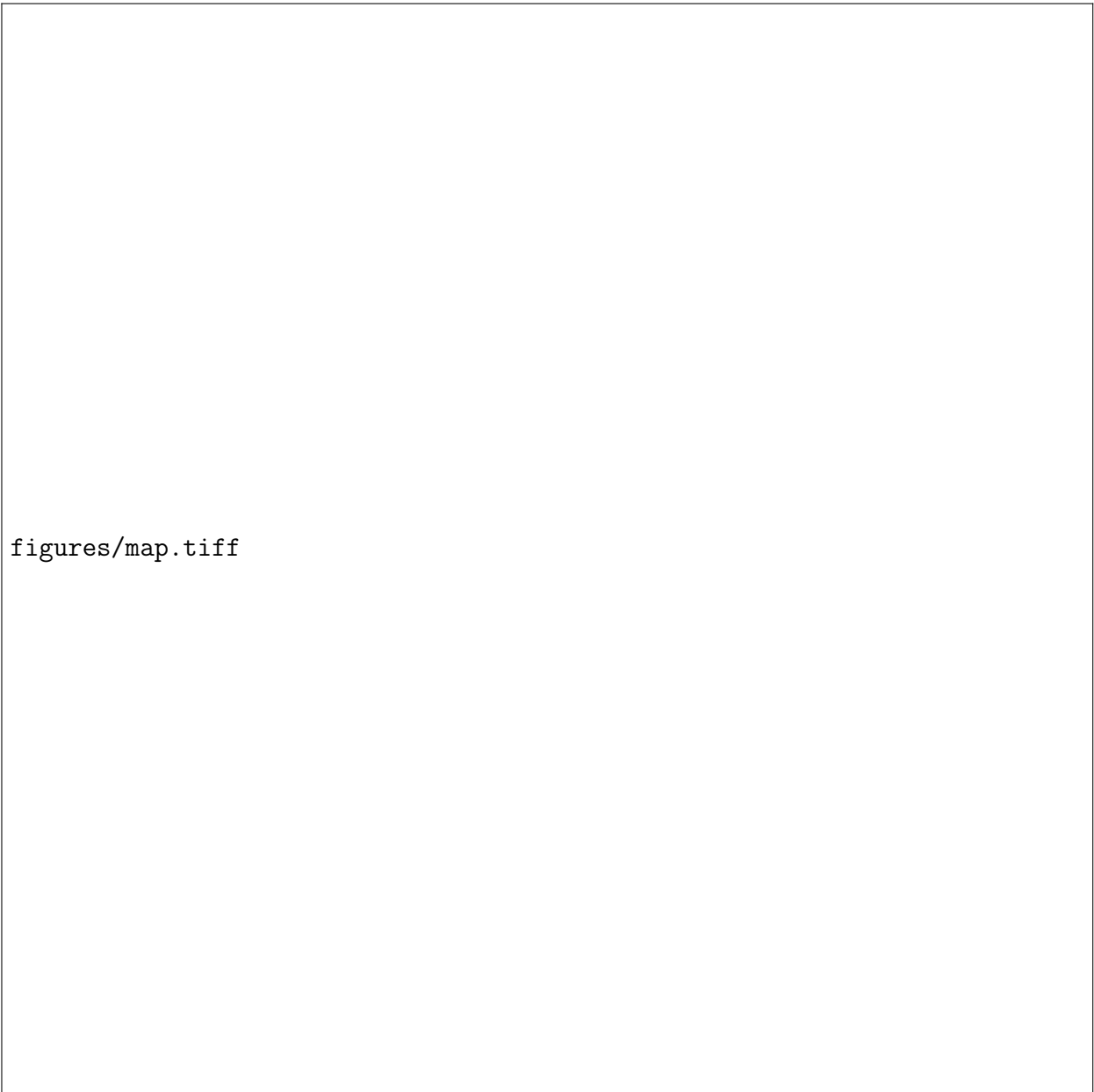
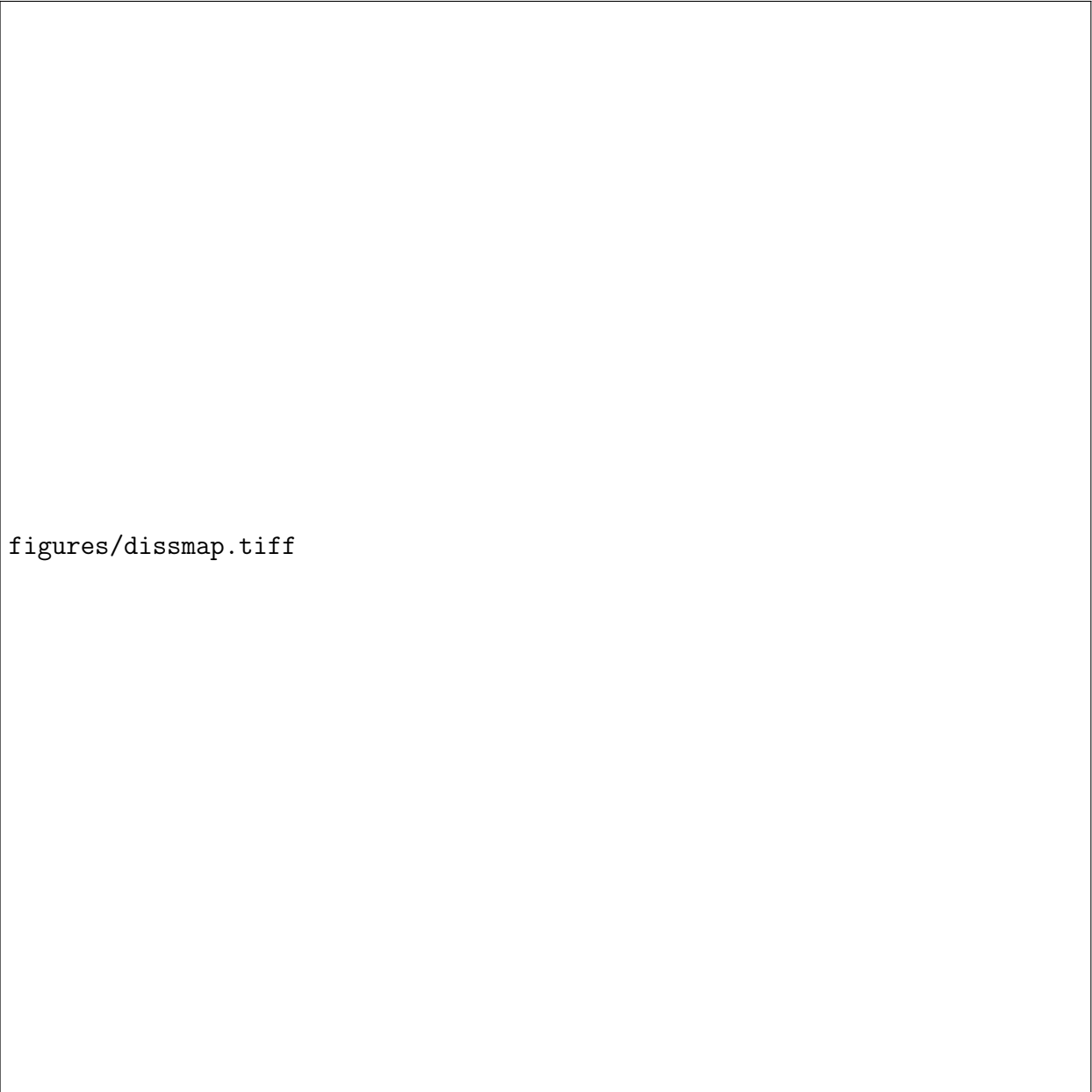


Figure 1. Bottom topography of the North Atlantic basin for the two boundary regions. Current meter locations considered in our analysis are highlighted by black crosses. The solid contours enclose the regions in which the nearest current meter is within a single decorrelation scale.



figures/dissmap.tiff

Figure 2. Maps showing the geographic distribution of BBL dissipation in the two boundary regions.

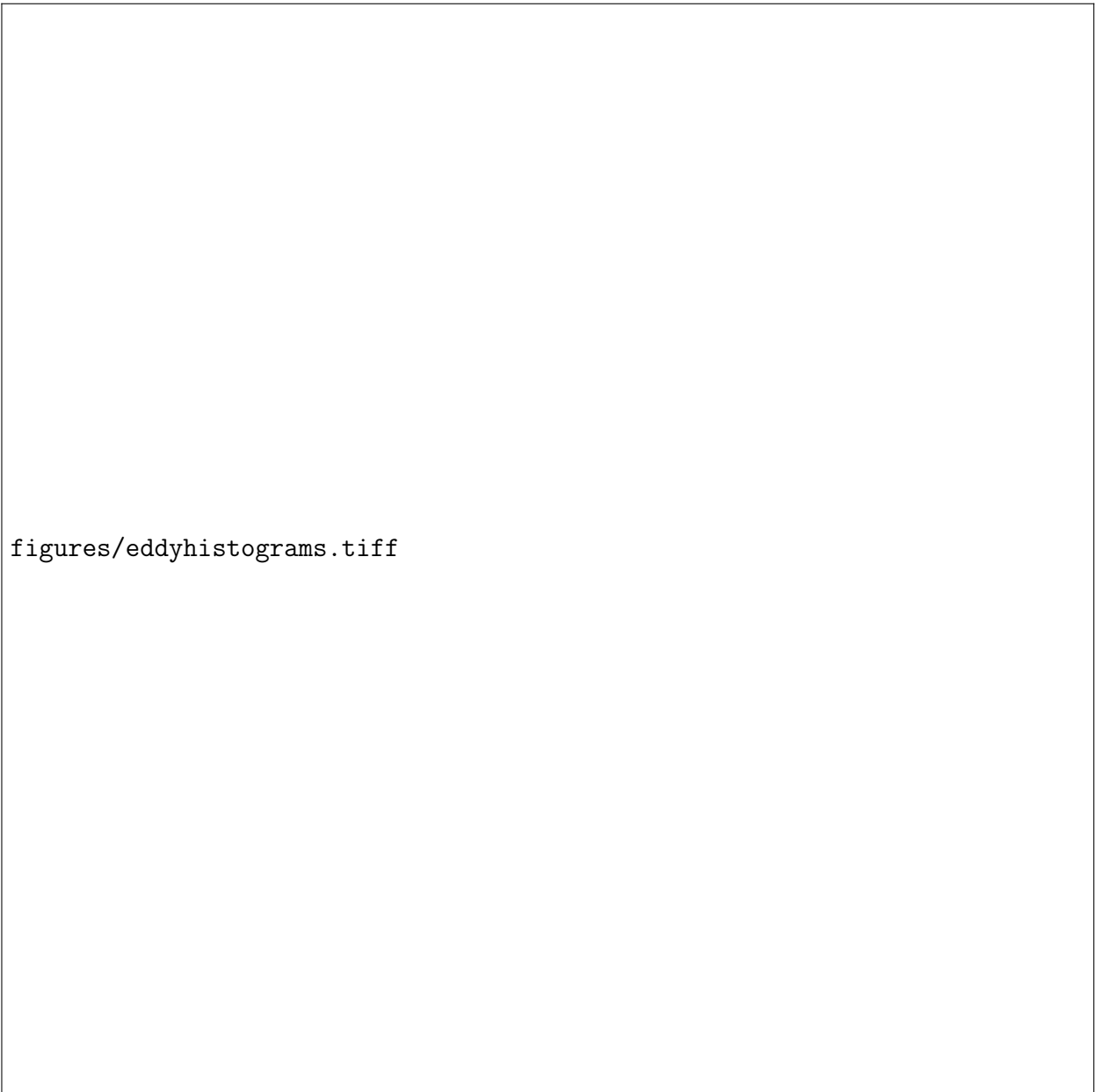


Figure 3. BBL dissipation as a function of depth. Wide bars indicate area on the right-hand scale, narrow bars the total BBL dissipation on the inner left-hand scale, and the curve the BBL dissipation per unit area on the outer left-hand scale. Note the different scales on each figure.